

## Microstructure and Preferred Grain Growth of Chemical Vapor Deposited ZrB<sub>2</sub> Coatings: Post-print

**Authors:** Zhang Jun, Zhang Lei, Guodong Li, Xiong Xiang

**Date:** 2017-04-10T00:00:00+00:00

### Abstract

Using ZrCl<sub>4</sub>-BCl<sub>3</sub>-H<sub>2</sub>-Ar as the chemical vapor deposition reaction system, ZrB<sub>2</sub> coatings were deposited at different temperatures, and the microstructure morphology and preferred grain growth of the coatings were characterized by X-ray diffraction and scanning electron microscopy (SEM). The results show that: on the graphite substrate surface, the nucleation mode of ZrB<sub>2</sub> coating is island growth; the continuous generation and coalescence of islands, along with grain growth, result in the coating near the graphite substrate surface containing numerous pores and forming a fine-grained zone. In the early stage of deposition at 1300~1600°C, primary grains in the ZrB<sub>2</sub> coating fuse into secondary grains, exhibiting preferred growth in the <111> direction. As deposition proceeds, the morphology of the ZrB<sub>2</sub> coating evolves from secondary grains to plate-like grains; plate-like grains further grow and transform into a pyramid morphology, the interior of the coating grows into dense columnar crystals, and the preferred orientation of grains transitions from <111> to <100>; when the edges of pyramid-shaped grains become blunted, grains within the coating transform into equiaxed crystals, and the preferred orientation of grains changes from the <100> direction to the <101> direction.

### Full Text

#### Preamble

Vol. 31 No. 3  
March 2017

#### CHINESE JOURNAL OF MATERIALS RESEARCH

#### Micro-Morphology and Preferential Growth of ZrB<sub>2</sub> Coating Prepared by Chemical Vapor Deposition

ZHANG Jun, ZHANG Lei, LI Guodong, XIONG Xiang  
(State Key Laboratory of Powder Metallurgy, Central South University, Changsha 410083, China)

Correspondent: LI Guodong, Tel: 13087317973, E-mail: lgd63@163.com  
Supported by National Program on Key Basic Research Project of China (No. 2011CB605805)  
Manuscript received 2016-04-29, in revised form 2016-10-11

---

## Abstract

ZrB<sub>2</sub> coating was deposited on graphite by chemical vapor deposition using ZrCl<sub>4</sub>-BCl<sub>3</sub>-H<sub>2</sub>-Ar as the reaction system at different temperatures, and the coating microstructure and preferential grain growth were characterized by X-ray diffraction and scanning electron microscopy (SEM). The results show that the nucleation mode of ZrB<sub>2</sub> coating on graphite substrate follows island growth. The continuous formation and merging of islands, together with grain growth, resulted in numerous pores in the coating near the graphite substrate surface, forming a fine-grained zone. During the initial deposition stage at 1300-1600°C, primary grains in the ZrB<sub>2</sub> coating coalesced into secondary grains, exhibiting preferential growth in the <111> direction. As deposition progressed, the morphology evolved from secondary grains to plate-shaped grains, which further developed into pyramid-shaped grains. The interior of the coating grew into dense columnar crystals, with the preferential orientation shifting from <111> to <100>. When the edges of pyramid-shaped grains became blunted, the interior grains transformed to equiaxed crystals, and the preferential orientation changed from <100> to <101>.

**KEY WORDS:** surface and interface in materials, ZrB<sub>2</sub> coating, chemical vapor deposition, micro morphology, orientation

---

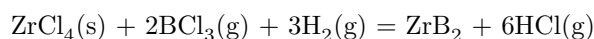
## Introduction

Zirconium diboride (ZrB<sub>2</sub>) exhibits high melting point, high hardness, high thermal and electrical conductivity, excellent corrosion resistance and oxidation resistance, and superior high-temperature mechanical properties, leading to widespread applications [1-4]. ZrB<sub>2</sub> demonstrates outstanding ablation resistance, with its oxidation products protecting the substrate material. As an excellent ultra-high temperature thermal protection coating material, ZrB<sub>2</sub> can be applied to rocket engine components, space reentry vehicles, and hypersonic vehicle thermal protection systems [5,6].

Preparation methods for ZrB<sub>2</sub> coatings mainly include brush coating [7], pack cementation [8-10], plasma spraying [11-12], and magnetron sputtering [13]. Com-

pared with these methods, chemical vapor deposition (CVD) offers easier control of coating structure and greater suitability for industrial applications. Deng Juanli investigated the thermodynamic and kinetic processes of chemical vapor deposition in the Zr-B-H-Cl reaction system within the temperature range of 900–1450 K [14]; A. Wang studied the surface morphology and deposition process of  $\text{ZrB}_2$  coatings at 1323–1473 K [15]. These studies demonstrate that growth conditions significantly influence the surface morphology and preferential growth of CVD-prepared  $\text{ZrB}_2$  coatings, with deposition temperature being a critical parameter affecting nucleation and growth during the CVD process. This work investigates the micro-morphology and preferential grain growth of  $\text{ZrB}_2$  coatings deposited at temperatures ranging from 1300°C to 1600°C.

The deposition substrates used in experiments were graphite plates measuring 30 mm × 20 mm × 5 mm with a density of 1.75 g/cm<sup>3</sup>. The substrates were polished with 800-grit sandpaper, cleaned with alcohol, and dried before use. The overall reaction for the  $\text{ZrCl}_4$ - $\text{BCl}_3$ - $\text{H}_2$ -Ar CVD system is:



where Ar served as a diluent gas and  $\text{H}_2$  as a reducing gas.  $\text{BCl}_3$  was the boron source with a vaporization temperature of 12.5°C. To eliminate environmental temperature fluctuations, the  $\text{BCl}_3$  source container was maintained at a constant temperature of 40°C using a water bath.  $\text{ZrCl}_4$  (99.9% purity) was the zirconium source, a light yellow solid powder. An adjustable powder feeding device was used to deliver it into the reaction zone, controlling the  $\text{ZrCl}_4$  powder flow rate to maintain uniformity [17]. The experimental process parameters are listed in .

Sample mass was measured using an Adventure<sup>TM</sup> electronic balance with 0.1 mg precision. Coating preferential orientation and phase composition were analyzed using a D/max2550VB+ 18 kW rotating target X-ray diffractometer (XRD). Coating morphology was observed using a NONA-SEM230 field emission scanning electron microscope (SEM).

---

## 2. Results and Discussion

### 2.1 X-ray Diffraction Analysis

[Figure 1: see original paper] shows the XRD patterns of  $\text{ZrB}_2$  coatings deposited at different temperatures. The analysis reveals that coatings deposited at various temperatures consist primarily of  $\text{ZrB}_2$  phase with sharp peaks, indicating good crystallinity. Coatings deposited at 1300°C and 1400°C exhibited extremely weak graphite peaks in their patterns. As deposition temperature increased, the graphite peaks disappeared. These graphite peaks originated from the substrate influence. With increasing deposition temperature, coating thickness increased, preventing X-rays from penetrating to the substrate, thus eliminating the graphite peaks.

As deposition temperature increased, coating thickness grew, and notably, the intensity ratios of different crystal planes changed. At 1300°C, the (100) plane showed the highest peak intensity, while (101) and (110) were relatively low. At 1400–1500°C, the (100) plane maintained the highest intensity, followed by the (110) plane. At 1500–1600°C, the intensities of (100) and (110) planes decreased, while the (101) plane relatively increased. Overall, as deposition temperature increased from 1300°C to 1600°C, the highest peak intensity shifted from the (100) plane to the (101) plane. These variations in peak intensities among different crystal planes indicate that the preferential orientation of grains in ZrB<sub>2</sub> coatings changes with temperature.

This change can be characterized using texture coefficients (TC). Applying the Harris formula [18], the relationship between texture coefficients of (100), (110), and (111) crystal planes and deposition temperature was calculated, as shown in [Figure 2: see original paper].

[Figure 2: see original paper] reveals that for the coating deposited at 1300°C, the texture coefficient is highest in the <100> direction, with relatively lower values in the <110> and <101> directions. As deposition temperature increased to 1400°C, the texture coefficient in the <110> direction increased, while that in the <101> direction decreased. When temperature further increased to 1500°C, texture coefficients in both <100> and <110> directions showed decreasing trends, while the <101> direction reached its minimum. At 1500–1600°C, the <101> texture coefficient increased sharply, the <110> direction decreased rapidly, and the <100> direction decreased slowly at first then rapidly. In summary, coatings deposited at different temperatures exhibit distinct preferential orientations, and these orientations change with increasing temperature. The coating deposited at 1500°C shows the most obvious change in preferential orientation, with <110> and <100> directions beginning to decline while the <101> direction starts to rise sharply.

## 2.2 Coating Surface Morphology

[Figure 3: see original paper] presents the surface morphologies of coatings deposited at different temperatures, where [Figure 3: see original paper]f shows an enlarged view of area A marked in [Figure 3: see original paper]e. At lower deposition temperatures such as 1300°C, the coating surface consisted primarily of spherical primary particles that interconnected and fused to form larger secondary particles without obvious crystallographic features. Overall, the coating contained numerous pores, as indicated by circular marks in [Figure 3: see original paper]a. As deposition temperature increased to 1400°C, particles further grew into plate-shaped grains. These grains fused with each other, developing incomplete edges and showing more pronounced textural characteristics, as marked by squares in [Figure 3: see original paper]b; pores remained abundant, as shown by circular marks in [Figure 3: see original paper]b. With further temperature increase, plate-shaped grains fused more extensively and continued growing, developing pyramid-shaped particles with incomplete pyramid forma-

tion, as indicated by triangular marks in [Figure 3: see original paper]c; surface pores began to decrease. At 1550°C, complete pyramid-shaped grains and plate-shaped grains stacked and fused tightly. The pyramid-shaped grains grew further, with some edges becoming blunted and edge angles exceeding 90°, as marked by ellipses in [Figure 3: see original paper]d. At 1600°C, pyramid-shaped grains grew larger, with individual grain edge angles significantly greater than 90°, as shown in [Figure 3: see original paper]f. [Figure 3: see original paper]e and [Figure 3: see original paper]f reveal that large grains fused with numerous small particles. After reaction completion at 1600°C, rapid cooling prevented residual reaction gas from being removed in time, and extensive nucleation at lower temperatures produced these particles on the coating surface.

Combining [Figure 1: see original paper] and [Figure 3: see original paper], at 1300°C, nuclei formed on the coating surface through Ostwald ripening to create larger secondary particles, with preferential growth primarily in the  $\langle 100 \rangle$  direction while  $\langle 101 \rangle$  and  $\langle 110 \rangle$  directions grew slower. As deposition temperature increased to 1400°C, secondary particles further grew into irregular plate-shaped grains, with preferential orientation dominated by  $\langle 100 \rangle$  followed by  $\langle 110 \rangle$ . As plate-shaped grains gradually developed completely and transformed toward pyramid morphology, preferential orientation remained dominated by  $\langle 100 \rangle$  while the  $\langle 110 \rangle$  direction relatively decreased. With further temperature increase, pyramid-shaped grain edges became blunted, and the  $\langle 101 \rangle$  preferential orientation increased significantly.

### 2.3 Coating Cross-Section Morphology

[Figure 4: see original paper] shows the cross-section morphologies of coatings deposited at different temperatures. As deposition temperature increased, pores in the coating gradually decreased and eventually disappeared, as marked by circles in [Figure 4: see original paper]a, b, c. At lower deposition temperature (1300°C), interior particles fused but with poor coalescence. Small grain morphologies remained visible on the natural fracture surface, and clear textural features could be observed inside the coating, as marked by rectangles in [Figure 4: see original paper]a. At 1400°C, particle fusion improved, grain morphology on the fracture surface became less distinct than at 1300°C, and pore numbers decreased significantly. At 1500°C, only extremely small pores remained, and the coating exhibited distinct upper (A) and lower (B) regions, as marked in [Figure 4: see original paper]c. The upper layer (A) consisted of dense columnar crystal zones with indistinct columnar morphology, while the lower layer (B) was a fine-grained particulate zone containing numerous pores. Particles were larger near the upper columnar crystal zone and smaller near the substrate. The lower layer (B) showed no obvious change with temperature increase. As deposition temperature continued to increase (1550°C), obvious columnar crystal features appeared in the upper layer (A), as shown in [Figure 4: see original paper]d. Further temperature increase caused columnar grains to grow and develop equiaxed characteristics, as shown in [Figure 4: see original

paper]e.

Combining [Figure 3: see original paper] and [Figure 4: see original paper], at 1300°C, extensive nucleation occurred on the coating surface with simultaneous Ostwald ripening forming secondary grains. Interior grains grew with textural characteristics, and numerous pores existed both on the surface and inside the coating. At 1400°C, nucleation became less pronounced, and coating growth was dominated by grain growth. As deposition temperature increased to 1500°C, grain fusion intensified, pores largely disappeared, and grain growth began forming columnar structures with well-densified grain boundaries. At 1550°C, distinct crystallographic features appeared on grain surfaces. Further temperature increase caused columnar crystals to transform toward equiaxed crystals.

Coating growth conditions significantly influence microstructure and preferential orientation. In the CVD process, primary growth conditions include deposition temperature, precursor ratio, and deposition pressure, with deposition temperature having the greatest impact on nucleation and growth processes. As shown in [Figure 5: see original paper], at lower deposition temperatures, adsorption, reaction, and migration rates on the substrate surface are relatively low, and the deposition process is primarily controlled by surface processes. Under constant other conditions, lower deposition temperature (1300°C) results in lower critical nucleation free energy, increasing the number of nuclei formed. Higher deposition temperature increases the size of critical nuclei and raises the critical free energy barrier for nucleation. Meanwhile, surface process rates increase, adsorption and desorption become more pronounced, the deposition process becomes controlled by gas molecular diffusion, and accelerated chemical reaction rates reduce supersaturation of the reaction system at the coating surface, making nucleation difficult and decreasing nucleation rate. As deposition temperature increases, vapor atom deposition, surface diffusion, and diffusion rates within the coating increase, grain aggregation and fusion intensify, and the coating formation mechanism transitions to grain growth-dominated.

According to droplet nucleation theory, the stability condition for core shapes during coating formation requires the following relationship between interfacial energies [19]:

$$\gamma_{\{vf\}} \cos \theta = \gamma_{\{sv\}} - \gamma_{\{fs\}}$$

Since  $\text{ZrB}_2$  has poor wettability with graphite substrate, the contact angle is large, and  $\gamma_{\{sv\}} < \gamma_{\{fs\}} + \gamma_{\{vf\}}$ . Based on these conditions, the nucleation mechanism of  $\text{ZrB}_2$  coating follows an island growth mode. During the initial deposition stage of  $\text{ZrB}_2$  coating, island-grown nuclei on the substrate surface continuously receive new deposited atoms and merge with other islands to form larger grains. Simultaneously, new islands continuously form on exposed substrate surfaces. This continuous island formation, merging, and grain growth leads to pore formation, creating a fine-grained zone containing numerous pores near the coating/substrate interface, as shown in [Figure 4: see

original paper]c. As deposition proceeds and coating thickness increases, more grains become shadowed by neighboring grains. Those grains with the fastest growth directions continue to grow preferentially, demonstrating preferential orientation in grain growth.

Previous studies [20,21] have established relationships between preferential grain orientation and crystal morphology in coatings, as summarized in , where  $\alpha$  represents the ratio of growth rates in different directions. shows that grain growth first forms cubes, then develops into octahedra. Combining [Figure 1: see original paper], [Figure 3: see original paper], and [Figure 4: see original paper], the following transformations occur from the coating surface to interior at deposition temperatures of 1300–1500°C: Nucleation continuously occurs on the coating surface, with new nuclei having random orientations, but smaller nuclei are swallowed by faster-growing grains or randomly fuse with other small grains, corresponding to [Figure 3: see original paper]a. This swallowing process has certain orientation preference ( $\langle 111 \rangle$ ), while small grain fusion is random. This grain swallowing allows faster-growing grains to first develop into cubic morphology with preferential  $\langle 111 \rangle$  plane growth. The plate-shaped grains in [Figure 3: see original paper]b represent incompletely grown cubic grains. Cubic grains continue growing and transform toward octahedral morphology, corresponding to the pyramid-shaped grains in [Figure 3: see original paper]c and d. During this process,  $\langle 110 \rangle$  planes grow preferentially. When interior grains transform to octahedral morphology, the (100) plane shows the highest peak intensity. Meanwhile, as deposition temperature increases from 1300°C to 1500°C, grain growth becomes dominant. During the transformation from cubic to octahedral morphology, grains in the coating grow preferentially in the  $\langle 100 \rangle$  direction while  $\langle 110 \rangle$  growth is suppressed. At 1500–1600°C, edges of octahedral grains become blunted, with some edge angles exceeding 90°. This edge blunting indicates that grains begin preferential growth in the  $\langle 101 \rangle$  direction, suppressing  $\langle 100 \rangle$  growth, and grain morphology further develops toward dodecahedral crystals.

According to Machlin' s theory on thin film texture [22], during the initial deposition stage, crystal planes with minimum surface energy drive grain growth, manifesting as  $\langle 111 \rangle$  preferential orientation in  $\text{ZrB}_2$  coating deposition. Grain growth processes and mismatch with the substrate inevitably generate internal stress within the coating. This internal stress continuously increases with coating thickness, and partial stress release creates defects such as sub-twin crystals and stacking faults within grains, providing new nucleation sites at grain boundaries. When internal stress release exceeds the increase in crystal plane surface energy, the anisotropy of internal stress promotes grain growth along crystal planes with lower strain energy. During  $\text{ZrB}_2$  deposition, the preferential orientation changes from  $\langle 111 \rangle$  to  $\langle 100 \rangle$ , corresponding to the morphology transition from plate-shaped to pyramid-shaped grains. The change from  $\langle 100 \rangle$  to  $\langle 101 \rangle$  preferential orientation corresponds to the blunting of pyramid-shaped grain edges.

---

## Conclusions

- (1) ZrB<sub>2</sub> coating formation on graphite substrate follows an island growth nucleation mode. The continuous formation and merging of islands, together with grain growth, create numerous pores near the substrate surface, forming a fine-grained zone.
- (2) At deposition temperatures of 1300-1600°C, during the initial deposition stage, primary grains in the ZrB<sub>2</sub> coating coalesce into secondary grains, exhibiting preferential growth in the <111> direction. As deposition progresses, the morphology evolves from secondary grains to plate-shaped grains. Plate-shaped grains further grow and transform into pyramid-shaped grains, while the interior develops dense columnar crystals. The preferential orientation shifts from <111> to <100>. When pyramid-shaped grain edges become blunted, interior grains transform to equiaxed crystals, and the preferential orientation changes from <100> to <101>.

---

## References

- [1] S. H. Jung, H.C. Oh, J. H. Kim, et al. Pretreatment of zirconium diboride powder to improve densification[J]. *J. Alloys Compd.*, 2013, 548(1): 173
- [2] Opeka M M, Talmy I G, Zaykoski J A, et al. Oxidation-based materials selection for 2000°C+hypersonic aero surfaces: theoretical considerations and historical experience[J]. *Mater Sci.*, 2004, 39(19):
- [3] Fahrenholtz W G, Hilmas G E, Refractory diborides of zirconium and hafnium[J]. *Am Ceram Soc.*, 2007, 90(5): 1347
- [4] Parthasarathy T A, Rapp R A, Opeka M, et al. A model for the oxidation of ZrB<sub>2</sub>, HfB<sub>2</sub> and TiB<sub>2</sub>[J]. *Acta Mater.*, 2007, 55(17):
- [5] C. Q. Liu, K. Z. Lin, H. J. Li, et al. In situ synthesis mechanism of ZrB<sub>2</sub>-ZrC-C composites[J], *Ceram. Int*, 2014, 40(40): 10297
- [6] X. Ren, H. J. Li, Y. H. Chu, et al., Preparation of oxidation protective ZrB<sub>2</sub>-SiC coating by in-situ reaction method on SiC-coated carbon/carbon composites[J]. *Surf. Coat. Technol*, 2014, 247(5): 61
- [7] Zhao D, Zhang C R, Zhang Y D, et al., Reactive preparation and properties of ZrB<sub>2</sub> coating [J]. *J. Inorg Mater*, 2011, 26(9): 903 (Zhao Dan, Zhang Changrui, Zhang Yudi, et al. Reactive preparation of zirconium diboride ultra-high temperature resistant coating. *Journal of Inorganic Materials*[J], 2011, 26(9): 903)
- [8] H J Zhou, G Le, W Zhen, et al. ZrB<sub>2</sub>-SiC Oxidation Protective Coating on C/C Composites Prepared by Vapor Silicon Infiltration Process[J]. *Am Ceram Soc*, 2010, 93(4): 915
- [9] X Zou, Q G Fu, L Liu, et al. ZrB<sub>2</sub>-SiC coating to protect carbon/carbon composites against ablation[J]. *Surf. Coat. Technol*, 2013, 226(14): 17

- [10] X Yang, W Li, S Wang, et al., ZrB<sub>2</sub> coating for the oxidation protection of carbon fiber reinforced silicon carbide matrix composites[J]. Vacuum, 2013, 96(10): 63
- [11] Rupa P K P, Sharma P, Mohanty R M, et al. Microstructure and phase composition of composite coatings formed by plasma spraying of ZrO<sub>2</sub> and B<sub>4</sub>C powders[J]. J. Therm. Spray. Technol, 2010, 19(4): 816
- [12] X Y Yao, H J Li, Y L Zhang, et al., Ablation behavior of ZrB<sub>2</sub>-based coating prepared by supersonic plasma spraying for SiC-coated C/C composites under oxyacetylene[J]. J. Therm. Spray. Technol, 2013, 22(4): 531
- [13] D J Li, M X Wang, J J Zhang, Structural and mechanical responses of (Zr, Al)N/ZrB<sub>2</sub> superlattice coatings to elevated-temperature annealing [J]. Mater. Sci. Eng, 2006, 423(1): 116
- [14] J L Deng, L F Cheng, G P Zheng, et al. Thermodynamic study on co-deposition of ZrB<sub>2</sub>-SiC from ZrCl<sub>4</sub>-BCl<sub>3</sub>-CH<sub>3</sub>SiCl<sub>3</sub>-H<sub>2</sub>-Ar system. Thin Solid Films, 2012, 520(23): 7030
- [15] A Wang, G Male. Experimental system investigation of the Zr-B-Cl-H CVD[J]. J. Eur Ceram. Soc, 1993, 11(3): 241
- [16] Chen Q Y, Liu S J, Physical Chemistry [M]. Beijing: Science Press, 2012 (Chen Qiyuan, Liu Shijun. Physical Chemistry[M]. Beijing: Science Press, 2012)
- [17] Li G D, Xiong X, Liu G, et al. Adjustable uniform powder feeder [P]. CHINA, 201010538190, 2010 (Li Guodong, Xiong Xiang, Liu Gang, et al. Adjustable uniform powder feeder[P]. China, 201010538190, 2010)
- [18] R. Y. Korotkov, P. Ricol, A. J. E. Farran. Preferred orientations in polycrystalline SnO<sub>2</sub> films grown by atmospheric pressure chemical vapor deposition[J]. Thin Solid Films, 2006, 502(1): 79
- [19] Chen Q Y, Liu Z J. Physical Chemistry [M]. Beijing: Science Press, 2012 (Chen Qiyuan, Liu Shijun. Physical Chemistry[M]. Beijing: Science Press, 2012)
- [20] K. L. Bjorklund, J. Lu, P. Heszler, et al., Kinetics, thermodynamics and microstructure of tungsten rods grown by thermal laser CVD[J]. Thin Solid Films, 2002, 416(1): 41
- [21] P. Smereka, X. Q. Li, G. Russo, et al, Simulation of faceted film growth in three dimensions: Microstructure, morphology and texture[J]. Acta Mater, 2005, 53(4): 1191
- [22] E. S Machlin., Materials science in microelectronics[M]. New York: Giro Press, 1995

*Note: Figure translations are in progress. See original paper for figures.*

*Source: ChinaXiv – Machine translation. Verify with original.*